Atmospheric
Chemistry
and Physics
Discussions

Open Access

Heterogeneous ice nucleation of viscous secondary organic aerosol produced from ozonolysis of α-pinene

K. Ignatius[1], T. B. Kristensen[1], E. Järvinen[2], L. Nichman[3], C. Fuchs[4],
H. Gordon[5], P. Herenz[1], C. R. Hoyle[4,6], J. Duplissy[7], S. Garimella[8], A. Dias[5],
C. Frege[4], N. Höppel[2], J. Tröstl[4], R. Wagner[7], C. Yan[7], A. Amorim[9],
U. Baltensperger[4], J. Curtius[10], N. M. Donahue[11], M. W. Gallagher[3], J. Kirkby[5,10],
M. Kulmala[7], O. Möhler[2], H. Saathoff[2], M. Schnaiter[2], A. Tomé[12], A. Virtanen[13],
D. Worsnop[14], and F. Stratmann[1]

[1]Leibniz Institute for Tropospheric Research (TROPOS), 04318 Leipzig, Germany
[2]Institute of Meteorology and Climate Research – Atmospheric Aerosol Research, Karlsruhe Institute of Technology, Karlsruhe, Germany
[3]School of Earth, Atmospheric and Environmental Sciences, University of Manchester, Manchester, M13 9PL, UK
[4]Laboratory of Atmospheric Chemistry, Paul Scherrer Institute, Villigen, Switzerland
[5]CERN, 1211 Geneva, Switzerland
[6]WSL Institute for Snow and Avalanche Research SLF Davos, Switzerland
[7]Department of Physics, P.O. Box 64, 00014 University of Helsinki, Finland

Discussion Paper | Discussion Paper | Discussion Paper | Discussion Paper |

ACPD

15, 35719–35752, 2015

Ice nucleation of viscous α-pinene SOA

K. Ignatius et al.

Title Page

Abstract | Introduction

Conclusions | References

Tables | Figures

|◄ | ►|

◄ | ►

Back | Close

Full Screen / Esc

Printer-friendly Version

Interactive Discussion

[8]Massachusetts Institute of Technology, Cambridge, MA, USA
[9]SIM/CENTRA and F. Ciencias, Universidade de Lisboa, Lisboa, Portugal
[10]Goethe-University of Frankfurt, Institute for Atmospheric and Environmental Sciences, Altenhöferallee 1, 60438 Frankfurt am Main, Germany
[11]Center for Atmospheric Particle Studies, Carnegie Mellon University, Pittsburgh, PA 15213, USA
[12]SIM/IDL, Universidade da Beira Interior, Covilhã, Portugal
[13]Department of Applied Physics, University of Eastern Finland, Kuopio, Finland
[14]Aerodyne Research, Inc., Billerica, MA 08121, USA

Correspondence to: K. Ignatius (ignatius@tropos.de)

Title Page

Abstract	Introduction
Conclusions	References
Tables	Figures

|◄ | ►|

◄ | ►

Back | Close

Full Screen / Esc

Printer-friendly Version

Interactive Discussion

Abstract

There are strong indications that particles containing secondary organic aerosol (SOA) exhibit amorphous solid or semi-solid phase states in the atmosphere. This may facilitate deposition ice nucleation and thus influence cirrus cloud properties. However, experimental ice nucleation studies of biogenic SOA are scarce. Here, we investigated the ice nucleation ability of viscous SOA particles.

The SOA particles were produced from the ozone initiated oxidation of α-pinene in an aerosol chamber at temperatures in the range from −38 to −10 °C at 5–15 % relative humidity with respect to water to ensure their formation in a highly viscous phase state, i.e. semi-solid or glassy. The ice nucleation ability of SOA particles with different sizes was investigated with a new continuous flow diffusion chamber. For the first time, we observed heterogeneous ice nucleation of viscous α-pinene SOA in the deposition mode for ice saturation ratios between 1.3 and 1.4 significantly below the homogeneous freezing limit. The maximum frozen fractions found at temperatures between −36.5 and −38.3 °C ranged from 6 to 20 % and did not depend on the particle surface area. Global modelling of monoterpene SOA particles suggests that viscous biogenic SOA particles are indeed present in regions where cirrus cloud formation takes place. Hence, they could make up an important contribution to the global ice nuclei (IN) budget.

1   Introduction

Atmospheric aerosol particles are known to influence the Earth's radiative balance and climate directly by reflecting and absorbing sunlight, and indirectly through their influence on clouds, e.g. when the particles act as cloud condensation nuclei (CCN) and/or ice nuclei (IN) (Yu et al., 2006). Determining the role of aerosols in ice nucleation is particularly complex because of different pathways through which ice forms in the atmosphere. Ice nucleation can be either homogeneous – freezing of pure water or

solute droplets – or heterogeneous, in which case ice formation is induced by foreign surfaces such as e.g. mineral dust or bacteria (Pruppacher and Klett, 1997). Homogeneous ice nucleation requires temperatures below approximately $-37\,°C$ and high supersaturations, typically ice saturation ratios S_{ice} of 1.4 or larger (Koop et al., 2000),
5 and contributes to cirrus cloud formation.

Heterogeneous ice nucleation is considered to be an important pathway for ice formation in the troposphere, especially in mixed-phase clouds (Krämer et al., 2009; Cziczo et al., 2013). Immersion freezing of aerosol particles activated into supercooled cloud droplets is the most important process for primary ice formation down to temper-
10 atures of around $-35\,°C$. Deposition ice nucleation, on the other hand, is more relevant at lower temperatures, and the typical IN inducing deposition nucleation are different mineral dusts, such as clay minerals and Saharan dust (DeMott et al., 2003; Möhler et al., 2006; Welti et al., 2009; Hoose and Möhler, 2012). DeMott et al. (2010) found that only about 1 in 10^5 or 10^6 atmospheric aerosol particles can act as an IN. In het-
15 erogeneous ice nucleation, the surface area of the seed particles typically plays an important role so that the larger particles tend to be more efficient IN (Connolly et al., 2009; Welti et al., 2009).

Secondary organic aerosol (SOA) can exist in a semi-solid, amorphous state in the atmosphere, and it has been suggested that these SOA particles could play a role in
20 ice nucleation (Zobrist et al., 2008; Virtanen et al., 2010). SOA is produced in the atmosphere from oxidation and subsequent condensation of volatile organic compounds (VOCs) (Hallquist et al., 2009) of which the majority are biogenic (Guenther et al., 1995; Jimenez et al., 2009). SOA is very abundant especially in the lower troposphere where it comprises around 30 to 70 % of the submicron particulate mass (Kanakidou
25 et al., 2005). Monoterpenes such as α-pinene are one of the most common biogenic SOA precursors, especially in boreal forest regions (Laaksonen et al., 2008). Other precursors include e.g. limonene in Australian Eucalyptus forests (Suni et al., 2007) and isoprene (Guenther et al., 2006).

The phase state of SOA depends on temperature and relative humidity (RH) (Zobrist et al., 2008) and has recently received more attention, since it determines the impact of SOA on cloud formation and therefore climate (Renbaum-Wolff et al., 2013). Depending on particle hygroscopicity, the viscosity of SOA is RH dependent; e.g. SOA produced from ozonolysis of α-pinene is known to take up water at high relative humidities (Pajunoja et al., 2015). Since humidity conditions vary significantly in the troposphere, SOA particles may exhibit many different phase states during their lifetime in the atmosphere. Ice particle residuals from cirrus clouds sampled in situ were rich in oxidized organic matter (Froyd et al., 2009, 2010), which indicates that viscous or glassy organic particles may also have acted as IN during cirrus formation. Modelling studies suggest that viscous SOA could be an important IN especially at low temperatures and low humidities, i.e. in the cirrus regime (Koop et al., 2011; Adler et al., 2013; Berkemeier et al., 2014). Furthermore, experimental studies of the ice nucleation ability of viscous SOA proxies support the model findings. In chamber expansion studies, citric acid, raffinose and levoglucosan particles nucleated ice heterogeneously at temperatures between −50 and −80 °C (Murray et al., 2010; Wagner et al., 2012; Wilson et al., 2012). Sucrose, glucose and citric acid particles were found to be very efficient INs in the deposition mode at temperatures between −70 and −40 °C since they nucleated ice at low ice saturation ratios (S_{ice} = 1.1) (Baustian et al., 2013). Simulated SOA from aqueous phase reactions of methylglyoxal and methylamine have also shown ice nucleation potential in the deposition mode (Schill et al., 2014).

Amorphous SOA particles generated via gas-phase oxidation of naphthalene with OH radicals are considered relatively efficient IN (Wang et al., 2012). Ladino et al. (2014) and Möhler et al. (2008) reported SOA produced from ozonolysis of α-pinene to be a poor or inefficient IN. In both studies, however, the phase state of SOA particles was not investigated experimentally, and the particles were produced at room temperature in a separate aerosol preparation chamber from which a fraction of them was transferred to the actual ice nucleation chamber. Thus, it is likely that the particles had such a low viscosity that they liquified before freezing homogeneously. Ladino

et al. (2014) also pointed out that precooling of the α-pinene SOA particles made them slightly better IN, possibly due to a change in viscosity.

Here, we report first observations of deposition ice nucleation of laboratory generated viscous, semi-solid α-pinene SOA. The phase state of the SOA particles was detected via the depolarisation signal of light scattered from the particles, using a novel optical method described in detail in a companion study (Järvinen et al., 2015). A new portable IN counter was used to sample the SOA particles and measure their ice nucleation efficiency. Finally, a global model was applied to investigate to what extent viscous SOA particles could contribute to the global IN budget.

2 Methods

2.1 Experimental setup: chamber experiments

The SOA particles were produced in the CLOUD (Cosmics Leaving Outdoor Droplets) chamber at CERN (Duplissy et al., 2010, 2015; Kirkby et al., 2011) during the CLOUD9 campaign between 25 October and 3 November 2014. SOA particles were produced from ozonolysis of α-pinene at low relative humidity with respect to water (RH_w) (5–15 %) at 4 different temperatures, −10, −20, −30 and −38 °C, which are relevant for the free troposphere. α-pinene and ozone were introduced to the chamber at the rate of 10 and 1000 mL min^{-1} (respectively) over a time period of a few minutes. UV lights (Philips TUV 130 W XPT lamp) were on during this time, resulting in the photolysis of O_3 and OH formation. High number concentrations of particles ($> 10^5$ cm^{-3}) quickly formed a monomodal size distribution which grew to approximately 100 nm in diameter. During the particle growth, α-pinene and ozone were continually introduced into the chamber. The particles were grown to approximately 600–800 nm in diameter in order to follow the size-dependence of their optical properties. The depolarisation ratio was measured, and based on the determined depolarisation of the incident light, it was determined that the particles were aspherical and thus viscous. Then the RH_w

Full Screen / Esc

Printer-friendly Version

Interactive Discussion

was slowly increased for the optical detection of the phase transition of the particles from viscous to liquid at the point where the depolarisation ratio decreased. The transition RH_w increased with the decreasing temperature, from 35 % at −10 °C to 80 % at −38 °C. Further experimental details are explained in Järvinen et al. (2015). The ice nucleation ability of the SOA particles was measured by sampling them from the CLOUD chamber at different growth stages in order to examine particles with different sizes. In Table 1 the particle size and concentrations for the different experiments are included together with information about the chamber temperature and humidity conditions. The particle number size distributions were measured with several Scanning Mobility Particle Sizer (SMPS) systems (20–800 nm), and optically with an Ultra High Sensitivity Aerosol Spectrometer (UHSAS, Droplet Measurement Technologies, Inc.) in the range from 60 nm to 1 µm. In addition, an Aerodyne high-resolution time-of-flight aerosol mass spectrometer (HR-ToF AMS) was used to determine the chemical composition of the SOA particles.

2.2 Ice nucleation instrumentation

We used the Spectrometer for Ice Nuclei (SPIN) to measure the ice nucleation efficiency of the SOA particles generated in the CLOUD chamber. SPIN is a new, commercially available portable IN counter manufactured by Droplet Measurement Technologies, Inc. It is a continuous flow diffusion chamber with parallel plate geometry adapted from the design of the Portable Ice Nucleation Chamber PINC (Chou et al., 2011) and the Zurich Ice Nucleation Chamber ZINC (Stetzer et al., 2008). The aerosol sample flow was set to 1 L min^{-1} surrounded by a sheath flow of 10 L min^{-1} through a chamber where a supersaturation of water vapour with respect to ice is obtained by keeping two ice covered walls at different temperatures below 0 °C. The residence time in the upper part of the chamber where ice nucleation may take place is then approximately 10 s. The aerosol sample is then exposed to an isothermal, separately temperature-controlled evaporation section where the unfrozen droplets evaporate while the ice particles are retained, prior to particle detection with a linear polarisation optical parti-

cle counter (OPC). The OPC laser is polarised, and the intensity of the backscattered light perpendicular to the incident polarisation and the intensity of backscattered polarised light are measured on a particle by particle basis. The polarisation-equivalent ratio between the two intensities provides information about the phase state of the particles. The size measurements of the SPIN OPC were calibrated using glass beads in the size range from 0.5 to 11.4 μm. The lower detection limit of the SPIN OPC was approximately 400 nm, with a detection efficiency of ∼ 50 %. For particles larger than 700 nm, the detection efficiency was close to 100 %. For particle sizes between 550 and 600 nm, the detection efficiency was approximately 80 %. This allows the SPIN OPC to detect also the seed aerosol particles if they are large enough.

The temperature of the aerosol sample flow and the supersaturation with respect to ice are modelled based on the continuous measurement of the wall temperatures. Due to a temperature gradient between the walls, there is a buoyancy effect to the air mass inside the chamber, pushing the sample flow closer to the colder wall. This effect has been taken into account in the 1-D-modelling and calculations of sample temperature and humidity which are done according to Rogers (1988). A Condensation Particle Counter (CPC-3720, TSI) was run parallel to SPIN during half of the runs, when the sample particle size was smaller than 500 nm. Due to limitations in the cooling system and temperature control of SPIN, the regime of operation for the current study was limited to a minimum temperature of −43 °C for the colder wall. SPIN was operated by keeping the colder wall at constant temperature at its lower limit and ramping up the temperature of the warm wall, thus raising the sample temperature from −40 to −35 °C and ice saturation ratio S_{ice} from 1 to 1.45–1.5 inside the instrument.

SPIN sampled the SOA particles from the CLOUD chamber through a 1.5 m long, quarter inch stainless steel tubing, in which the residence time was approximately 2 s. As the concentrations of the SOA particles in the CLOUD chamber typically exceeded 10 000 cm^{-3}, a dilution system partly filtering away aerosol particles was used to dilute the sample so that the particle number concentrations entering SPIN would stay under 1000 cm^{-3} in order to avoid saturating the optical detector. The stainless steel tubing

together with the dilution system was insulated, but the temperature of the sample was not continually measured at the SPIN inlet, and it is possible that the temperature in the sampling tube was higher than in the CLOUD chamber.

2.3 Instrument performance validation by homogeneous freezing of highly diluted ammonium sulphate droplets

Homogeneous freezing of highly diluted ammonium sulphate droplets was used to validate the performance of the SPIN chamber and the optical detector. Ammonium sulphate particles were generated from a 1.0 mass % solution with a medical nebulizer, dried in a diffusion dryer and then size-selected by a Differential Mobility Analyser (DMA). Mean mobility diameters of 200 and 500 nm were chosen, and a CPC (CPC-3010, TSI) was run in parallel to measure the total particle concentration.

The freezing experiments were designed in the following way: first a supersaturation with respect to ice and water was created inside SPIN by diverging the wall temperatures in order to obtain the necessary temperature gradient, while keeping the sample temperature below −37 °C, which is the upper threshold temperature for homogeneous freezing in the atmosphere (Pruppacher and Klett, 1997). After water (super)saturation was achieved and ice formation observed, both walls were heated at the same rate in order to the increase the sample temperature but keep the water supersaturation, leading to the disappearance of ice. The temperature of the evaporation section walls was kept constant at −35 °C.

An example of such an experiment is displayed in Fig. 1. In the upper left panel, the SPIN wall and sample (lamina) temperatures, as well as the relative humidity with respect to liquid water are plotted as a function of time. The upper right panel shows the particle number concentrations in different size bins from the same experiment. At subsaturated conditions with respect to liquid water only the 500 nm seed aerosol particles are observed. When water saturation is reached shortly after 14.3 h, most of the seeds activate to droplets which then freeze, forming a distinct mode with sizes around

5 µm. As the sample temperature is increased, the ice mode vanishes at approximately 14.4 h and a mode consisting of liquid droplets with sizes of ∼ 2–3 µm remains.

In the lower three panels of Fig. 1, the raw size distributions from the same experiment corresponding to each observed mode are shown. Panel (a) shows the dry 500 nm seed aerosol particles that have not yet activated. Panel (b) illustrates the situation when most of the ammonium sulphate particles have activated into droplets and frozen. Panel (c) depicts the seed aerosol and liquid, highly diluted ammonium sulphate droplets at water supersaturation at temperatures above the homogeneous freezing point. All the data are normalised with respect to total particle counts from the OPC. The polarisation-equivalent ratios (S/P ratios) from the OPC are also different for ice crystals and liquid droplets: for ice, S/P ratios vary between 0.5 and 0.6, whereas for liquid droplets the ratios are significantly smaller, between 0.1 and 0.2. This further confirms that the distinct modes in the size distributions correspond to different phase states, and the size distributions can also be used to define ice nucleation onset points.

The homogeneous freezing temperatures for a frozen fraction of 10 % are shown in Fig. 2. The homogeneous freezing temperatures are all found in the range from −37.9 to −36.6 °C, with an average value of −37.3 °C. The variation in S_{ice} comes from using slightly different temperature gradients to introduce a supersaturation with respect to water inside SPIN. Based on classical nucleation theory and the parameterisation of homogeneous nucleation rates of water presented by Ickes et al. (2015), a frozen fraction of 10 % can be expected for a temperature in the range from about −38.2 to −37.6 °C. Uncertainties and variations in the residence time and the sizes of droplets formed inside SPIN results in the uncertainty in the expected homogeneous freezing temperature. Hence, the homogeneous freezing temperatures reported in Fig. 2 are within the range or slightly higher than what could be expected from theory. However, with a temperature difference between the SPIN chamber walls close to 20 °C, the aerosol sample temperature range is approximately ±0.4 °C with respect to the average temperatures presented in Fig. 2. Roughly half of the droplets formed inside SPIN

will thus be exposed to temperatures down to ∼ 0.4 °C below the average aerosol sample temperature.

The freezing point depression caused by ammonium sulphate in the water droplets was calculated using the following formula:

$$\Delta T = iM \times 1.86,\tag{1}$$

where i is the van't Hoff factor of the solute, M is the molar concentration of the solution, and $1.86\,\text{km}^{-1}$ is the freezing point depression for an ideal solution (Seinfeld and Pandis, 2006). For ammonium sulphate, $i = 2.04$ (Wu et al., 2011). The droplet diameter here was estimated to be 3 μm. For 200 nm ammonium sulphate particles, this solute effect is negligible ($\Delta T = 0.015$ °C); for 500 nm particles the freezing point depression is 0.24 °C, which is still within the uncertainty range of the aerosol sample temperature inside SPIN. Thus, we can conclude that the droplets were dilute enough so that the presense of ammonium sulphate did not significantly influence the freezing temperature.

With all the uncertainties considered, the correspondence between theory and experimentally obtained homogeneous freezing temperatures with SPIN is good, with a systematic tendency of the experimental temperatures being slightly too high (≲0.5 °C). This off-set is likely to be due to occasional locally slightly colder chamber wall sections in between thermocouples relative to the temperature set-points. Based on the results presented in Fig. 2 it can be concluded that the aerosol sample conditions inside SPIN can be reproduced with a high accuracy between different experiments, and the inferred aerosol sample conditions correspond well to what can be expected from theory.

3 Results and discussion

Here, we present results from deposition ice nucleation measurements, on viscous α-pinene SOA, obtained with SPIN. First, we show size distributions in order to dis-

tinguish deposition nucleation from homogeneous freezing. Then, frozen fractions and ice activation conditions are presented, as well as a comparison to literature data. Atmospheric implications of the results will be discussed in the end of the section.

3.1 Size distributions

Figure 3 shows results of a typical deposition ice nucleation ramp with viscous SOA particles; this example is from 26 October 2014. Analogously to Fig. 1, the middle three panels show particle number size distributions observed during the deposition ice nucleation ramp, and a size distribution from an experiment, when the RH with respect to liquid water was greater than 100 %. The latter experiment was performed in order to investigate droplet breakthrough, i.e. at which RH a fraction of the formed liquid droplets remain as droplets after the SPIN evaporation section. The leftmost panel (a) shows the 550 nm seed aerosol and the middle panel (b) depicts the seeds and ice (a size mode around 5 µm) at water subsaturated conditions. A prominent liquid droplet mode can be seen in the third panel (c), when the RH_w was greater than 100 % and part of the liquified particles froze homogeneously. Also here, there was a clear difference in the polarisation-equivalent S/P ratios between the liquid droplets and ice, as can be seen from the bottom three panels.

3.2 Frozen fractions

The fraction of particles activated as ice crystals was defined as the number of particles larger than the minimum between the seed aerosol and ice crystal modes, or between the liquid droplet and ice modes, divided by the total number of particles. In the case of SOA particles, this threshold size was 3 µm. It cannot be ruled out, however, that there is some size overlap between ice crystals and liquid droplets, since due to the design of SPIN, not all particles nucleate ice at the same time and not all the droplets necessarily evaporate in the evaporation section.

We investigated different SOA particle sizes from 120 nm to approximately 800 nm (see Table 1 for details). Figure 4 shows exemplary frozen fractions of 330, 550 and 800 nm viscous SOA particles as a function of the ice saturation ratio. The 330 nm particles were produced in the CLOUD chamber at −38 °C, and at the time of ice formation the temperature inside SPIN was −37.7 ± 0.4 °C. The 550 nm particles were produced at −20 °C, and nucleated ice at −38.1±0.4 °C; the 800 nm particles produced at −10 °C nucleated ice at −37.0±0.4 °C. The maximum frozen fractions observed were ∼ 6–20 % but they did not show any clear dependency on the seed particle size; nor did the 1 % ice activation onset values, although there is some variation among the different particle sizes.

SOA particle properties relevant for ice nucleation could depend on the chemical composition and morphology, which could depend on the chamber conditions. The mean atomic oxygen to carbon ratio (O : C) of the SOA particles inferred from AMS measurements was 0.25 throughout the different stages of the different experiments (Järvinen et al., 2015): this would suggest possibly similar chemical composition of the particles throughout the experiments. The apparent similarity in the chemical composition for different SOA particle sizes does not explain why there is no significant change in the frozen fraction or freezing onsets when the seed particles grow larger. Surface area dependency has previously been shown for deposition ice nucleation of different mineral dusts by Welti et al. (2009), but there is no indication of such a dependency for the viscous SOA particles studied here.

3.3 Ice nucleation onset conditions for viscous SOA

Ice nucleation onset conditions were defined as the temperature and ice saturation ratio when the activated (frozen) fraction of SOA particles was 1 %. Figure 5 shows the ice nucleation onsets for viscous *α*-pinene SOA in the deposition and homogeneous freezing mode. The error bars of the deposition nucleation data are calculated from the statistical standard deviation σ, and represent the 95 % confidence interval (1.96σ) in both temperature and supersaturation. An estimate for the instrumental temperature

uncertainty was ±1 °C on both walls inside the chamber; the statistical approach gives 1.07 °C as the error bar for temperature, which indicates that the conservative error estimate would also have been valid. Homogeneous freezing onset was observed only once, hence the error bars in supersaturation correspond to the theoretical maximum error calculated from the estimated instrumental temperature uncertainty. The uncertainty distribution of a theoretical maximum error is, however, unknown, and cannot be treated e.g. as Gaussian or evenly distributed.

Based on investigations of size distributions and the corresponding sample temperatures and humidities for several different experiments, it is qualitatively quite clear that the observed freezing facilitated by the viscous SOA particles occurs as deposition freezing at subsaturated conditions with respect to liquid water. However, the results were also analysed with statistical tools in order to test if the freezing occurred at subsaturated conditions with respect to liquid water. A paired t test (assuming a Gaussian distribution of the data) showed that the difference in saturation ratio between the data points and the saturation line with respect to liquid water is statistically significant ($p = 10^{-6}$). In a similar fashion the more robust Wilcoxon signed-rank test (Wilcoxon, 1945) confirmed a statistically significant difference ($p = 0.003$).

With the size distribution method presented here, we are able to distinguish heterogeneous ice nucleation from homogeneous freezing. From our measurements, we have strong evidence that highly viscous α-pinene SOA induces ice nucleation in the deposition mode. Despite intrumental limitations, the results were reproducible and the uncertainty for the ice nucleation onset temperatures and supersaturations could be inferred.

3.4   Comparison to literature data

Figure 6 shows our results together with selected literature data. The ice saturation ratios we have observed for the ice nucleation onset temperatures for viscous α-pinene SOA are qualitatively comparable with ice nucleation data from other SOA or SOA proxies, but the lack of data points at lower temperatures makes quantitative compari-

son challenging. There is notable difference between our results and those reported by Ladino et al. (2014) and Möhler et al. (2008), who found α-pinene SOA to be a poor IN. In Ladino et al. (2014), the SOA particles were produced in a smog chamber and a flow tube at room temperature and then either sampled directly, or collected on teflon filters and extracted in a solution, from which the particles were formed with an atomizer and dried prior to sampling. There was no significant difference in the ice nucleation behaviour between the freshly sampled particles and filter samples. Ladino et al. (2014) also found, however, that pre-cooling of the particles made them better IN, and interpret it as a result of a transition to a more viscous state, although the phase state of the particles was not studied experimentally. Thus, it is likely that the non-pre-cooled fresh particles and filter samples had a low viscosity and liquefied before ice activation in the ice nucleation chamber. In Möhler et al. (2008), the SOA particles were produced in a separate aerosol preparation chamber at room temperature, from which they were transferred to the cloud expansion chamber where they were exposed to $RH_w > 50\%$ at $-68\,°C$ before the experiments. Also here, the viscosity of the SOA particles was not investigated, and the particles did not nucleate ice in the deposition mode, but homogeneously, requiring high ice supersaturations.

In our case, the α-pinene SOA were freshly generated at subzero temperatures (from -10 to $-38\,°C$) and low RH_w (5–15 %), under conditions typical for upper troposphere, and sampled directly from the CLOUD chamber. In the companion study by Järvinen et al. (2015) it was experimentally observed that for these α-pinene SOA particles the transition timescales were of the order of tens of minutes. At $-38\,°C$ the transition happened around $RH_w = 80\%$; inside SPIN, the conditions at which deposition ice nucleation onset was observed were between $RH_w = 91\%$ and $RH_w = 97\%$. The deliquescence process from highly viscous semi-solid to liquid is not instantaneous, and depending on the temperature and the $O:C$ ratio, the particles may persist in a viscous state over long time periods, even of the order of days (Berkemeier et al., 2014). Since the total residence time in the sampling tube and SPIN was approximately 12 s, it is

Title Page

Abstract | Introduction

Conclusions | References

Tables | Figures

|◄ | ►|

◄ | ►

Back | Close

Full Screen / Esc

Printer-friendly Version

Interactive Discussion

likely that these SOA particles kept their highly viscous state even at higher humidities than the transition RH long enough to act as IN in the deposition mode.

When compared to other IN, such as different mineral dusts, viscous α-pinene SOA requires higher ice saturation ratios for 1 % activated fraction than e.g. kaolinite and illite at −35 and −40 °C (Welti et al., 2009). The maximum ice fractions, on the other hand, are of the same order of magnitude. The viscous SOA particles seem to be more efficient deposition mode IN than volcanic ash at −35 and −40 °C measured by Hoyle et al. (2011), with similar or lower ice saturation ratios needed for 1 % activation and higher maximum ice fractions.

3.5 Atmospheric implications

Viscous pinene SOA particles have already been observed in the lower troposphere in field measurements in the boreal forest (Virtanen et al., 2010). The global aerosol model GLOMAP-mode (GLObal Model of Aerosol Processes) (Mann et al., 2010) was used to investigate whether viscous biogenic monoterpene SOA is likely to be present in the atmosphere. The model version used is identical to that in Riccobono et al. (2014). GLOMAP is an extension to the TOMCAT chemical transport model (Chipperfield, 2006). It includes representations of particle formation, growth via coagulation, condensation and cloud processing, wet and dry deposition and in/below cloud scavenging. The horizontal resolution is $2.8° \times 2.8°$ and there are 31 vertical sigma-pressure levels extending from ground level to 10 hPa. Formation of secondary particles in the model is based on CLOUD measurements of ternary H_2SO_4-organic-H_2O nucleation detailed in Riccobono et al. (2014) and on a parameterisation of binary H_2SO_4-H_2O nucleation (Kulmala et al., 1998). Particles grow by irreversible condensation of monoterpene oxidation products and sulphuric acid. Monoterpene emissions in the model are taken from the Guenther et al. (1995) database. The monoterpenes are oxidised with OH, O_3 and NO_3 assuming the reaction rates of α-pinene. A fixed 13 % of the oxidation products, referred to as SORG, condenses irreversibly onto aerosol particles at the kinetic limit.

Figure 7 shows the mean annual average concentrations of SORG in parts per trillion with respect to mass (pptm). SORG represents oxidised monoterpenes and can in this respect be considered a proxy of monoterpene SOA particles. The hatched areas mark the zones in the atmosphere where the SOA particles are likely to exist in a highly viscous or even glassy phase state according to the generic estimate of SOA glass transition temperature as a function of relative humidity given by Koop et al. (2011). This parameterisation agrees with the viscosity transitions of the investigated α-pinene SOA particles that were measured in the CLOUD chamber simultaneously with the ice nucleation experiments (Järvinen et al., 2015; Nichman et al., 2015). At the lowest temperature ($-38\,°C$) the transition RH was observed to be even slightly higher (80 %) than predicted by Koop et al. (2011), indicating that at low temperatures the Koop et al. (2011) generic SOA glass transition temperature model may underestimate the number of viscous SOA particles (Järvinen et al., 2015).

The modelled monoterpene SOA proxy concentrations are highest over land and especially in the tropics, but near the equator the conditions for particles containing monoterpene SOA to be highly viscous require higher altitudes (~ 7 km) and colder temperatures (see Fig. 7 right panel). On the other hand, strong convective updrafts may play a role carrying the SOA particles even into the tropical tropopause layer (TTL) in short enough timescales for the particles to remain highly viscous (Berkemeier et al., 2014), or SOA may form in convective outflow regions, after the transport of precursor gases from lower altitudes in the troposphere. Boreal forests are a significant source of monoterpenes in spring and summertime of the Northern Hemisphere, and model calculations displayed in Fig. 7 indicate that sufficient concentrations of viscous monoterpene SOA could exist in the upper troposphere in this region, thus being a potential source of ice nuclei for cirrus cloud formation. It should be noted that particles with other types of SOA than α-pinene SOA may facilitate ice nucleation in cirrus clouds, or persist in a viscous state at higher temperatures or humidities (Berkemeier et al., 2014). The model results presented here nevertheless indicate qualitatively that significant concentrations of SOA-forming vapours are likely to exist in parts of the tro-

Ice nucleation of viscous α-pinene SOA

K. Ignatius et al.

Title Page

Abstract	Introduction
Conclusions	References
Tables	Figures

|◀ | ▶|

◀ | ▶

Back | Close

Full Screen / Esc

Printer-friendly Version

Interactive Discussion

posphere where the particles they form would be in a sufficiently viscous state to act as IN.

So far, SOA has not been considered in climate models involving ice nucleation, and it is still very challenging to quantify the actual effect, but given the potentially high ice nucleation efficiency (up to 20 % frozen fractions), α-pinene and other monoterpene SOA could contribute significantly to the global IN budget. It is likely that a significant portion of biogenic SOA in the atmosphere form mixtures with sulphates or primary particles such as mineral dusts; that will most likely also affect the ice nucleation efficiency considerably.

4   Conclusions

In this study, we produced viscous α-pinene SOA particles at 10 % RH at 4 different atmospherically relevant subzero temperatures, −10, −20, −30 and −38 °C, and measured their ice nucleation capability with a new portable IN counter. We have, for the first time, found a strong indication that viscous SOA produced from ozonolysis of α-pinene efficiently nucleates ice. We conducted reproducible measurements and applied a size distribution method to determine that the ice nucleation was heterogeneous and in the deposition mode. Homogeneous freezing was also observed when the conditions inside the portable IN chamber were at or above water saturation. We investigated SOA particles with mean diameters from 120 to 800 nm, and no dependency was observed between the particle size and the frozen fraction/freezing onset. The frozen fractions reached a maximum of ∼ 6–20 %. Ice saturation ratios for the observed ice nucleation onset temperatures are in line with previous literature data, but the range of observed ice nucleation onset temperatures was narrow due to instrumental limitations. Therefore further experimental studies are recommended.

To date, viscous or glassy biogenic SOA has not been considered as IN in any climate models. Here, results from a global aerosol model suggest that α-pinene SOA may exist at least regionally in considerable numbers in the upper troposphere in the

Discussion Paper | Discussion Paper | Discussion Paper | Discussion Paper | Discussion Paper |

ACPD

15, 35719–35752, 2015

Ice nucleation of viscous α-pinene SOA

K. Ignatius et al.

Title Page

Abstract | Introduction

Conclusions | References

Tables | Figures

|◄ | ►|

◄ | ►

Back | Close

Full Screen / Esc

Printer-friendly Version

Interactive Discussion

cirrus regime where they would be highly viscous or glassy. Thus boreal forests and other regions emitting monoterpenes could potentially be a significant source of IN contributing to the global IN budget. In order to better quantify the impact of highly viscous or glassy biogenic SOA as IN to the climate, extensive future experimental and modelling studies will be needed.

References

Adler, G., Koop, T., Haspel, C., Taraniuk, I., Moise, T., Koren, I., Heiblum, R. H., and Rudich, Y.: Formation of highly porous aerosol particles by atmospheric freeze-drying in ice clouds, P. Natl. Acad. Sci. USA, 110, 20414–20419, 2013. 35723

Baustian, K. J., Wise, M. E., Jensen, E. J., Schill, G. P., Freedman, M. A., and Tolbert, M. A.: State transformations and ice nucleation in amorphous (semi-)solid organic aerosol, Atmos. Chem. Phys., 13, 5615–5628, doi:10.5194/acp-13-5615-2013, 2013. 35723, 35751

Berkemeier, T., Shiraiwa, M., Pöschl, U., and Koop, T.: Competition between water uptake and ice nucleation by glassy organic aerosol particles, Atmos. Chem. Phys., 14, 12513–12531, doi:10.5194/acp-14-12513-2014, 2014. 35723, 35733, 35735

Chipperfield, M. P.: New version of the TOMCAT/SLIMCAT off-line chemical transport model: intercomparison of stratospheric tracer experiments, Q. J. Roy. Meteorol. Soc., 132, 1179–1203, 2006. 35734

Chou, C., Stetzer, O., Weingartner, E., Jurányi, Z., Kanji, Z. A., and Lohmann, U.: Ice nuclei properties within a Saharan dust event at the Jungfraujoch in the Swiss Alps, Atmos. Chem. Phys., 11, 4725–4738, doi:10.5194/acp-11-4725-2011, 2011. 35725

Connolly, P. J., Möhler, O., Field, P. R., Saathoff, H., Burgess, R., Choularton, T., and Gallagher, M.: Studies of heterogeneous freezing by three different desert dust samples, Atmos. Chem. Phys., 9, 2805–2824, doi:10.5194/acp-9-2805-2009, 2009. 35722

Cziczo, D. J., Froyd, K. D., Hoose, C., Jensen, E. J., Diao, M. H., Zondlo, M. A., Smith, J. B., Twohy, C. H., and Murphy, D. M.: Clarifying the dominant sources and mechanisms of cirrus cloud formation, Science, 340, 1320–1324, 2013. 35722

DeMott, P. J., Sassen, K., Poellot, M. R., Baumgardner, D., Rogers, D. C., Brooks, S. D., Prenni, A. J., and Kreidenweis, S. M.: African dust aerosols as atmospheric ice nuclei, Geophys. Res. Lett., 30, 1732, doi:10.1029/2003GL017410, 2003. 35722

DeMott, P. J., Prenni, A. J., Liu, X., Kreidenweis, S. M., Petters, M. D., Twohy, C. H., Richardson, M. S., Eidhammer, T., and Rogers, D. C.: Predicting global atmospheric ice nuclei distributions and their impacts on climate, P. Natl. Acad. Sci. USA, 107, 11217–11222, 2010. 35722

Duplissy, J., Enghoff, M. B., Aplin, K. L., Arnold, F., Aufmhoff, H., Avngaard, M., Baltensperger, U., Bondo, T., Bingham, R., Carslaw, K., Curtius, J., David, A., Fastrup, B., Gagné, S., Hahn, F., Harrison, R. G., Kellett, B., Kirkby, J., Kulmala, M., Laakso, L., Laaksonen, A., Lillestol, E., Lockwood, M., Mäkelä, J., Makhmutov, V., Marsh, N. D., Nieminen, T., Onnela, A., Pedersen, E., Pedersen, J. O. P., Polny, J., Reichl, U., Seinfeld, J. H., Sipilä, M., Stozhkov, Y., Stratmann, F., Svensmark, H., Svensmark, J., Veenhof, R., Verheggen, B., Viisanen, Y., Wagner, P. E., Wehrle, G., Weingartner, E., Wex, H., Wilhelmsson, M., and Winkler, P. M.: Results from the CERN pilot CLOUD experiment, Atmos. Chem. Phys., 10, 1635–1647, doi:10.5194/acp-10-1635-2010, 2010. 35724

Duplissy, J., Merikanto, J., Franchin, A., Tsagkogeorgas, G., Kangasluoma, J., Wimmer, D., Vuollekoski, H., Schobesberger, S., Lehtipalo, K., Flagan, R. C., Brus, D., Donahue, N. M., Vehkamäki, H., Almeida, J., Amorim, A., Barmet, P., Bianchi, F., Breitenlechner, M., Dunne, E. M., Guida, R., Henschel, H., Junninen, H., Kirkby, J., Kürten, A., A., K., Määttänen, A., Makhmutov, V., Mathot, S., Nieminen, T., Onnela, A., Praplan, A. P., Riccobono, F., Rondo, L., Steiner, G., Tomé, A., Walther, H., Baltensperger, U., Carslaw, K. S., Dommen, J., Hansel, A., Petäjä, T., Sipilä, M., Stratmann, F., Virtanen, A., Wagner, P. E., Worsnop, D. R., Curtius, J., and Kulmala, M.: Effect of ions on sulfuric acid-water binary particle formation II:

Ice nucleation of viscous α-pinene SOA

K. Ignatius et al.

Title Page

Abstract	Introduction
Conclusions	References
Tables	Figures

Back | Close

Full Screen / Esc

Printer-friendly Version

Interactive Discussion

Experimental data and comparison with QC-normalized classical nucleation theory, J. Geophys. Res., in press, doi:10.1002/2015JD023539, 2015. 35724

Froyd, K. D., Murphy, D. M., Sanford, T. J., Thomson, D. S., Wilson, J. C., Pfister, L., and Lait, L.: Aerosol composition of the tropical upper troposphere, Atmos. Chem. Phys., 9, 4363–4385, doi:10.5194/acp-9-4363-2009, 2009. 35723

Froyd, K. D., Murphy, D. M., Lawson, P., Baumgardner, D., and Herman, R. L.: Aerosols that form subvisible cirrus at the tropical tropopause, Atmos. Chem. Phys., 10, 209–218, doi:10.5194/acp-10-209-2010, 2010. 35723

Guenther, A., Hewitt, C. N., Erickson, D., Fall, R., Geron, C., Graedel, T., Harley, P., Klinger, L., Lerdau, M., Mckay, W. A., Pierce, T., Scholes, B., Steinbrecher, R., Tallamraju, R., Taylor, J., and Zimmerman, P.: A global model of natural volatile organic compound emissions, J. Geophys. Res.-Atmos., 100, 8873–8892, 1995. 35722, 35734

Guenther, A., Karl, T., Harley, P., Wiedinmyer, C., Palmer, P. I., and Geron, C.: Estimates of global terrestrial isoprene emissions using MEGAN (Model of Emissions of Gases and Aerosols from Nature), Atmos. Chem. Phys., 6, 3181–3210, doi:10.5194/acp-6-3181-2006, 2006. 35722

Hallquist, M., Wenger, J. C., Baltensperger, U., Rudich, Y., Simpson, D., Claeys, M., Dommen, J., Donahue, N. M., George, C., Goldstein, A. H., Hamilton, J. F., Herrmann, H., Hoffmann, T., Iinuma, Y., Jang, M., Jenkin, M. E., Jimenez, J. L., Kiendler-Scharr, A., Maenhaut, W., McFiggans, G., Mentel, Th. F., Monod, A., Prévôt, A. S. H., Seinfeld, J. H., Surratt, J. D., Szmigielski, R., and Wildt, J.: The formation, properties and impact of secondary organic aerosol: current and emerging issues, Atmos. Chem. Phys., 9, 5155–5236, doi:10.5194/acp-9-5155-2009, 2009. 35722

Hoose, C. and Möhler, O.: Heterogeneous ice nucleation on atmospheric aerosols: a review of results from laboratory experiments, Atmos. Chem. Phys., 12, 9817–9854, doi:10.5194/acp-12-9817-2012, 2012. 35722

Hoyle, C. R., Pinti, V., Welti, A., Zobrist, B., Marcolli, C., Luo, B., Höskuldsson, Á., Mattsson, H. B., Stetzer, O., Thorsteinsson, T., Larsen, G., and Peter, T.: Ice nucleation properties of volcanic ash from Eyjafjallajökull, Atmos. Chem. Phys., 11, 9911–9926, doi:10.5194/acp-11-9911-2011, 2011. 35734

Ickes, L., Welti, A., Hoose, C., and Lohmann, U.: Classical nucleation theory of homogeneous freezing of water: thermodynamic and kinetic parameters, Phys. Chem. Chem. Phys., 17, 5514–5537, 2015. 35728

Title Page

Abstract | Introduction

Conclusions | References

Tables | Figures

Back | Close

Full Screen / Esc

Printer-friendly Version

Interactive Discussion

Järvinen, E., Ignatius, K., Nichman, L., Kristensen, T. B., Fuchs, C., Höppel, N., Corbin, J. C., Craven, J., Duplissy, J., Ehrhart, S., El Haddad, I., Frege, C., Gates, S. J., Gordon, H., Hoyle, C. R., Jokinen, T., Kallinger, P., Kirkby, J., Kiselev, A., Naumann, K.-H., Petäjä, T., Pinterich, T., Prevot, A. S. H., Saathoff, H., Schiebel, T., Sengupta, K., Simon, M., Tröstl, J., Virtanen, A., Vochezer, P., Vogt, S., Wagner, A. C., Wagner, R., Williamson, C., Winkler, P. M., Yan, C., Baltensperger, U., Donahue, N. M., Flagan, R. C., Gallagher, M., Hansel, A., Kulmala, M., Stratmann, F., Worsnop, D. R., Möhler, O., Leisner, T., and Schnaiter, M.: Observation of viscosity transition in α-pinene secondary organic aerosol, Atmos. Chem. Phys. Discuss., 15, 28575–28617, doi:10.5194/acpd-15-28575-2015, 2015. 35724, 35725, 35731, 35733, 35735

Jimenez, J. L., Canagaratna, M. R., Donahue, N. M., Prevot, A. S. H., Zhang, Q., Kroll, J. H., DeCarlo, P. F., Allan, J. D., Coe, H., Ng, N. L., Aiken, A. C., Docherty, K. S., Ulbrich, I. M., Grieshop, A. P., Robinson, A. L., Duplissy, J., Smith, J. D., Wilson, K. R., Lanz, V. A., Hueglin, C., Sun, Y. L., Tian, J., Laaksonen, A., Raatikainen, T., Rautiainen, J., Vaattovaara, P., Ehn, M., Kulmala, M., Tomlinson, J. M., Collins, D. R., Cubison, M. J. E., Dunlea, J., Huffman, J. A., Onasch, T. B., Alfarra, M. R., Williams, P. I., Bower, K., Kondo, Y., Schneider, J., Drewnick, F., Borrmann, S., Weimer, S., Demerjian, K., Salcedo, D., Cottrell, L., Griffin, R., Takami, A., Miyoshi, T., Hatakeyama, S., Shimono, A., Sun, J. Y., Zhang, Y. M., Dzepina, K., Kimmel, J. R., Sueper, D., Jayne, J. T., Herndon, S. C., Trimborn, A. M., Williams, L. R., Wood, E. C., Middlebrook, A. M., Kolb, C. E., Baltensperger, U., and Worsnop, D. R.: Evolution of organic aerosols in the atmosphere, Science, 365, 1525–1529, 2009. 35722

Kanakidou, M., Seinfeld, J. H., Pandis, S. N., Barnes, I., Dentener, F. J., Facchini, M. C., Van Dingenen, R., Ervens, B., Nenes, A., Nielsen, C. J., Swietlicki, E., Putaud, J. P., Balkanski, Y., Fuzzi, S., Horth, J., Moortgat, G. K., Winterhalter, R., Myhre, C. E. L., Tsigaridis, K., Vignati, E., Stephanou, E. G., and Wilson, J.: Organic aerosol and global climate modelling: a review, Atmos. Chem. Phys., 5, 1053–1123, doi:10.5194/acp-5-1053-2005, 2005. 35722

Kirkby, J., Curtius, J., Almeida, J., Dunne, E., Duplissy, J., Ehrhart, S., Franchin, A., Gagne, S., Ickes, L., Kürten, A., Kupc, A., Metzger, A., Riccobono, F., Rondo, L., Schobesberger, S., Tsagkogeorgas, G., Wimmer, D., Amorim, A., Bianchi, F., Breitenlechner, M., David, A., Dommen, J., Downard, A., Ehn, M., Flagan, R. C., Haider, S., Hansel, A., Hauser, D., Jud, W., Junninen, H., Kreissl, F., Kvashin, A., Laaksonen, A., Lehtipalo, K., Lima, J., Lovejoy, E. R., Makhmutov, V., Mathot, S., Mikkilä, J., Minginette, P., Mogo, S., Nieminen, T., Onnela, A.,

Pereira, P., Petäjä, T., Schnitzhofer, R., Seinfeld, J. H., Sipilä, M., Stozhkov, Y., Stratmann, F., Tomé, A., Vanhanen, J., Viisanen, Y., Vrtala, A., Wagner, P. E., Walther, H., Weingartner, E., Wex, H., Winkler, P. M., Carslaw, K. E., Worsnop, D. R., Baltensperger, U., and Kulmala, M.: Role of sulphuric acid, ammonia and galactic cosmic rays in atmospheric aerosol nucleation, Nature, 476, 429–433, 2011. 35724

Koop, T., Luo, B., Tsias, A., and Peter, T.: Water activity as the determinant for homogeneous ice nucleation in aqueous solutions, Nature, 406, 611–614, 2000. 35722, 35747, 35751

Koop, T., Bookhold, J., Shiraiwa, M., and Pöschl, U.: Glass transition and phase state of organic compounds: dependency on molecular properties and implications for secondary organic aerosols in the atmosphere, Phys. Chem. Chem. Phys., 13, 19238–19255, 2011. 35723, 35735, 35752

Krämer, M., Schiller, C., Afchine, A., Bauer, R., Gensch, I., Mangold, A., Schlicht, S., Spelten, N., Sitnikov, N., Borrmann, S., de Reus, M., and Spichtinger, P.: Ice supersaturations and cirrus cloud crystal numbers, Atmos. Chem. Phys., 9, 3505–3522, doi:10.5194/acp-9-3505-2009, 2009. 35722

Kulmala, M., Laaksonen, A., and Pirjola, L.: Parameterizations for sulfuric acid/water nucleation rates, J. Geophys. Res., 103, 8301–8307, 1998. 35734

Laaksonen, A., Kulmala, M., O'Dowd, C. D., Joutsensaari, J., Vaattovaara, P., Mikkonen, S., Lehtinen, K. E. J., Sogacheva, L., Dal Maso, M., Aalto, P., Petäjä, T., Sogachev, A., Yoon, Y. J., Lihavainen, H., Nilsson, D., Facchini, M. C., Cavalli, F., Fuzzi, S., Hoffmann, T., Arnold, F., Hanke, M., Sellegri, K., Umann, B., Junkermann, W., Coe, H., Allan, J. D., Alfarra, M. R., Worsnop, D. R., Riekkola, M.-L., Hyötyläinen, T., and Viisanen, Y.: The role of VOC oxidation products in continental new particle formation, Atmos. Chem. Phys., 8, 2657–2665, doi:10.5194/acp-8-2657-2008, 2008. 35722

Ladino, L. A., Zhou, S., Yakobi-Hancock, J. D., Aljawhary, D., and Abbatt, J. P. D.: Factors controlling the ice nucleating abilities of α-pinene SOA particles, J. Geophys. Res.-Atmos., 119, 9041–9051, 2014. 35723, 35733, 35751

Mann, G. W., Carslaw, K. S., Spracklen, D. V., Ridley, D. A., Manktelow, P. T., Chipperfield, M. P., Pickering, S. J., and Johnson, C. E.: Description and evaluation of GLOMAP-mode: a modal global aerosol microphysics model for the UKCA composition-climate model, Geosci. Model Dev., 3, 519–551, doi:10.5194/gmd-3-519-2010, 2010. 35734

Möhler, O., Field, P. R., Connolly, P., Benz, S., Saathoff, H., Schnaiter, M., Wagner, R., Cotton, R., Krämer, M., Mangold, A., and Heymsfield, A. J.: Efficiency of the deposition mode ice

Ice nucleation of viscous α-pinene SOA

K. Ignatius et al.

Title Page

Abstract | Introduction

Conclusions | References

Tables | Figures

|◄ | ►|

◄ | ►

Back | Close

Full Screen / Esc

Printer-friendly Version

Interactive Discussion

nucleation on mineral dust particles, Atmos. Chem. Phys., 6, 3007–3021, doi:10.5194/acp-6-3007-2006, 2006. 35722

Möhler, O., Benz, S., Saathoff, H., Schnaiter, M., Wagner, R., Schneider, J., Walter, S., Ebert, V., and Wagner, S.: The effect of organic coating on the heterogeneous ice nucleation efficiency of mineral dust aerosols, Env. Res. Lett., 3, 025007, doi:10.1088/1748-9326/3/2/025007, 2008. 35723, 35733, 35751

Murray, B. J., Wilson, T. W., Dobbie, S., Cui, Z., Al-Jumur, S. M., Möhler, O., Schnaiter, M., Wagner, R., Benz, S., Niemand, M., Saathoff, H., Ebert, V., Wagner, S., and Kärcher, B.: Heterogeneous nucleation of ice particles on glassy aerosols under cirrus conditions, Nat. Geosci., 3, 233–237, 2010. 35723

Nichman, L., Fuchs, C., Järvinen, E., Ignatius, K., Höppel, N. F., Dias, A., Heinritzi, M., Simon, M., Tröstl, J., Wagner, A. C., Wagner, R., Williamson, C., Yan, C., Bianchi, F., Connolly, P. J., Dorsey, J. R., Duplissy, J., Ehrhart, S., Frege, C., Gordon, H., Hoyle, C. R., Kristensen, T. B., Steiner, G., Donahue, N. M., Flagan, R., Gallagher, M. W., Kirkby, J., Möhler, O., Saathoff, H., Schnaiter, M., Stratmann, F., and Tomé, A.: Discrimination of water, ice and aerosols by light polarisation in the CLOUD experiment, Atmos. Chem. Phys. Discuss., 15, 31433–31469, doi:10.5194/acpd-15-31433-2015, 2015. 35735

Pajunoja, A., Lambe, A. T., Hakala, J., Rastak, N., Cummings, M. J., Brogan, J. F., Hao, L., Paramonov, M., Hong, J., Prisle, N. L., Malila, J., Romakkaniemi, S., Lehtinen, K. E. J., Laaksonen, A., Kulmala, M., Massoli, P., Onasch, T. B., Donahue, N. M., Riipinen, I., Davidovits, P., Worsnop, D., Petäjä, T., and Virtanen, A.: Adsorptive uptake of water by semisolid secondary organic aerosols, Geophys. Res. Lett., 42, 3063–3068, 2015. 35723

Pruppacher, H. R. and Klett, J. D.: Microphysics of Clouds and Precipitation, Atmospheric and Oceanographic Sciences Library, Kluwer Academic Publishers, Dordrecht, the Netherlands, 1997. 35722, 35727

Renbaum-Wolff, L., Grayson, J., Bateman, A. P., Kuwata, K., Sellier, M., Murray, B. J., Schilling, J. E., Martin, S. T., and Bertram, A. K.: Viscosity of α-pinene secondary organic material and implications for particle growth and reactivity, P. Natl. Acad. Sci. USA, 110, 8014–8019, 2013. 35723

Riccobono, F., Schobesberger, S., Scott, C. E., Dommen, J., Ortega, I. K., Rondo, L., Almeida, J., Amorim, A., Bianchi, F., Breitenlechner, M., David, A., Downard, A., Dunne, E. M., Duplissy, J., Ehrhart, S., Flagan, R. C., Franchin, A., Hansel, A., Junninen, H., Kajos, M., Keskinen, H., Kupc, A., Kürten, A., Kvashin, A. N., Laaksonen, A., Lehtipalo, K.,

Ice nucleation of viscous α-pinene SOA

K. Ignatius et al.

Title Page

Abstract	Introduction
Conclusions	References
Tables	Figures

|◄ ►|

◄ ►

Back Close

Full Screen / Esc

Printer-friendly Version

Interactive Discussion

Makhmutov, V., Mathot, S., Nieminen, T., Onnela, A., Petäjä, T., Praplan, A. P., Santos, F. D., Schallhart, S., Seinfeld, J. H., Sipilä, M., Spracklen, D. V., Stozhkov, Y., Stratmann, F., Tomé, A., Tsagkogeorgas, G., Vaattovaara, P., Viisanen, Y., Vrtala, A., Wagner, P. E., Weingartner, E., Wex, H., Wimmer, D., Carslaw, K. S., Curtius, J., Donahue, N. M., Kirkby, J., Kulmala, M., Worsnop, D. R., and Baltensperger, U.: Oxidation products of biogenic emissions contribute to nucleation of atmospheric particles, Science, 344, 717–721, 2014. 35734

Rogers, D. C.: Development of a continuous flow thermal gradient diffusion chamber for ice nucleation studies, Atmos. Res., 22, 149–181, 1988. 35726

Schill, G. P., De Haan, D. O., and Tolbert, M. A.: Heterogeneous ice nucleation on simulated secondary organic aerosol, Environ. Sci. Technol., 48, 1675–1682, 2014. 35723

Seinfeld, J. H. and Pandis, S. N.: Atmospheric Chemistry and Physics: From Air Pollution to Climate Change, 2nd edn., John Wiley and Sons, Inc., Hoboken, New Jersey, USA, 2006. 35729

Stetzer, O., Baschek, B., Lüönd, F., and Lohmann, U.: The Zurich Ice Nucleation Chamber (ZINC) – a new instrument to investigate atmospheric ice formation, Aerosol Sci. Tech., 42, 64–72, 2008. 35725

Suni, T., Hakola, H., Bäck, J., Hurley, R., van Gorsel, E., Ruuskanen, T., Kulmala, M., Sogacheva, L., Leuning, R., Cleugh, H., and Keith, H.: Effect of vegetation on aerosol formation in South-East Australia, in: Nucleation and Atmospheric Aerosols, edited by: O'Dowd, C. D. and Wagner, P. E., Springer Netherlands, 1018–1022, 2007. 35722

Virtanen, A., Joutsensaari, J., Koop, T., Kannosto, J., Ylipirilä, P., Leskinen, J., Mäkelä, J. M., Holopainen, J. K., Pöschl, U., Kulmala, M., Worsnop, D. R., and Laaksonen, A.: An amorphous solid state of biogenic secondary organic aerosol particles, Nature, 467, 824–827, 2010. 35722, 35734

Wagner, R., Möhler, O., Saathoff, H., Schnaiter, M., Skrotzki, J., Leisner, T., Wilson, T. W., Malkin, T. L., and Murray, B. J.: Ice cloud processing of ultra-viscous/glassy aerosol particles leads to enhanced ice nucleation ability, Atmos. Chem. Phys., 12, 8589–8610, doi:10.5194/acp-12-8589-2012, 2012. 35723

Wang, B., Lambe, A. T., Massoli, P., Onasch, T. B., Davidovitsh, P., Worsnop, D. R., and Knopf, D. A.: The deposition ice nucleation and immersion freezing potential of amorphous secondary organic aerosol: pathways for ice and mixed-phase cloud formation, J. Geophys. Res.-Atmos., 117, D16209, doi:10.1029/2012JD018063, 2012. 35723, 35751

Title Page

Abstract | Introduction

Conclusions | References

Tables | Figures

|◄ | ►|

◄ | ►

Back | Close

Full Screen / Esc

Printer-friendly Version

Interactive Discussion

Welti, A., Lüönd, F., Stetzer, O., and Lohmann, U.: Influence of particle size on the ice nucleating ability of mineral dusts, Atmos. Chem. Phys., 9, 6705–6715, doi:10.5194/acp-9-6705-2009, 2009. 35722, 35731, 35734

Wilcoxon, F.: Individual comparisons by ranking methods, Biometrics Bull., 1, 80–83, 1945. 35732

Wilson, T. W., Murray, B. J., Wagner, R., Möhler, O., Saathoff, H., Schnaiter, M., Skrotzki, J., Price, H. C., Malkin, T. L., Dobbie, S., and Al-Jumur, S. M. R. K.: Glassy aerosols with a range of compositions nucleate ice heterogeneously at cirrus temperatures, Atmos. Chem. Phys., 12, 8611–8632, doi:10.5194/acp-12-8611-2012, 2012. 35723

Wu, Z. J., Nowak, A., Poulain, L., Herrmann, H., and Wiedensohler, A.: Hygroscopic behavior of atmospherically relevant water-soluble carboxylic salts and their influence on the water uptake of ammonium sulfate, Atmos. Chem. Phys., 11, 12617–12626, doi:10.5194/acp-11-12617-2011, 2011. 35729

Yu, H., Kaufman, Y. J., Chin, M., Feingold, G., Remer, L. A., Anderson, T. L., Balkanski, Y., Bellouin, N., Boucher, O., Christopher, S., DeCola, P., Kahn, R., Koch, D., Loeb, N., Reddy, M. S., Schulz, M., Takemura, T., and Zhou, M.: A review of measurement-based assessments of the aerosol direct radiative effect and forcing, Atmos. Chem. Phys., 6, 613–666, doi:10.5194/acp-6-613-2006, 2006. 35721

Zobrist, B., Marcolli, C., Pedernera, D. A., and Koop, T.: Do atmospheric aerosols form glasses?, Atmos. Chem. Phys., 8, 5221–5244, doi:10.5194/acp-8-5221-2008, 2008. 35722, 35723

Full Screen / Esc

Printer-friendly Version

Interactive Discussion

Table 1. The conditions for the ice nucleation experiments with viscous α-pinene SOA. The columns from left to right list the dates when the experiment was carried out, the average temperature in the CLOUD chamber during the particle sampling with the IN counter SPIN, the average relative humidity with respect to water RH_w in the CLOUD chamber, mean particle mobility diameters and the sampled particle number concentrations measured by the SPIN optical particle counter (OPC) and a Condensation Particle Counter (CPC). For each experiment, 1 to 4 ice nucleation onset measurements were performed. The CPC was operated parallel to SPIN during half of the runs. For the runs without CPC number concentrations, frozen fractions could be estimated from the SPIN OPC particle number concentrations and size distributions.

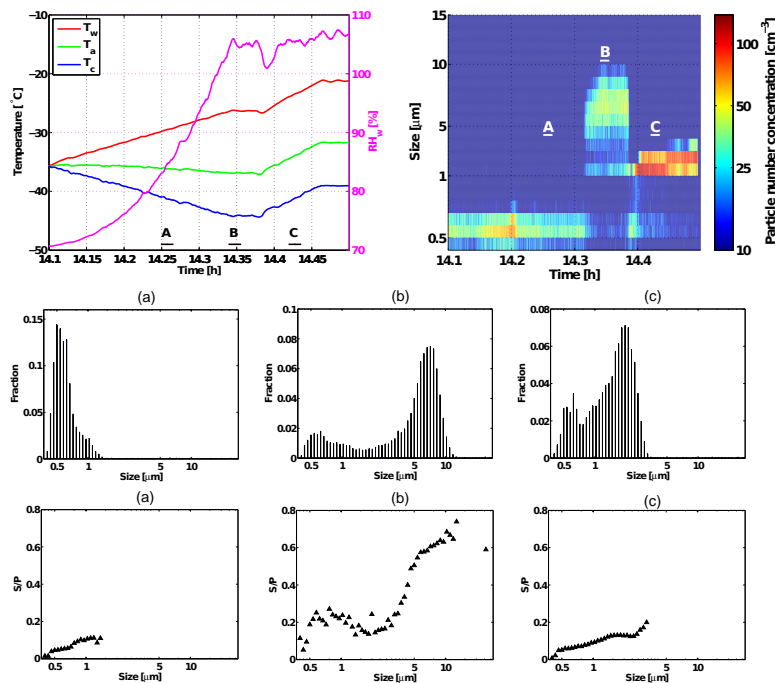| Date	Chamber T (°C)	Chamber RH_w (%)	Particle diameter (nm)	SPIN OPC conc. (cm^{-3})	CPC conc. (cm^{-3})
25 Oct	−10	12	800	200	–
26 Oct	−20	10	550, 600	150–600	–
27 Oct	−20	10	800	150	150
28 Oct	−30	10	320, 630	–	490
29 Oct	−38	10	330	–	310
3 Nov	−38	60	120	–	130

Figure 1. Homogeneous freezing of highly diluted ammonium sulphate droplets. In the top left panel, the SPIN cold and warm wall (T_c and T_w) and sample (lamina) temperatures (T_a), as well as the relative humidity with respect to liquid water (RH_w) are plotted as a function of time. The top right panel shows the particle number concentrations in different size bins from the same experiment. Bars A, B, C in the top panels mark the time intervals from which the normalised SPIN OPC particle number size distributions and the median values of the polarisation-equivalent S/P ratios are shown in the corresponding lower panels. In **(a)** seed particles, in **(b)** seed and ice particles, in **(c)** seed particles and liquid droplets. The size distributions and S/P ratios are averaged over 54 s, and correspond to the following times in the upper panels: **(a)** 14.25–14.265 h, **(b)** 14.34–14.355 h, **(c)** 14.42–14.435 h.
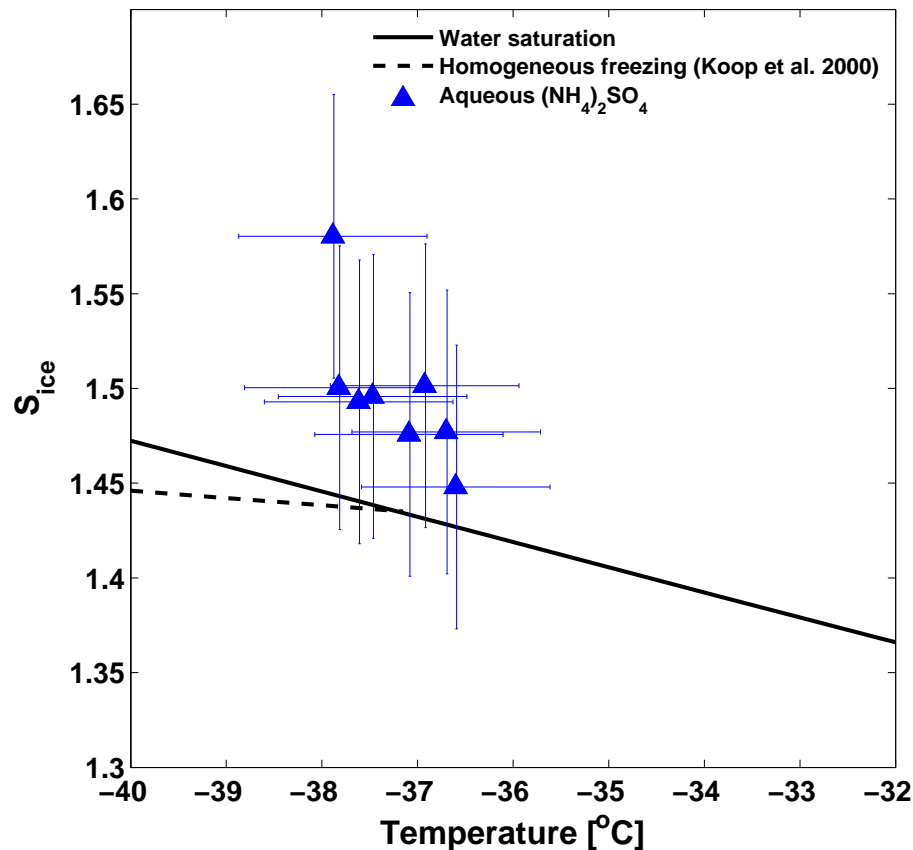
Figure 2. Homogeneous freezing temperatures of highly diluted ammonium sulphate droplets measured with SPIN. The frozen fraction here is 10 %. The uncertainties in temperature and ice saturation ratio shown here correspond to the 95 % confidence interval calculated from the statistical standard deviation. The homogeneous freezing line from Koop et al. (2000) is calculated for 500 nm particles.

Title Page

Abstract | Introduction

Conclusions | References

Tables | Figures

|◄ | ►|

◄ | ►

Back | Close

Full Screen / Esc

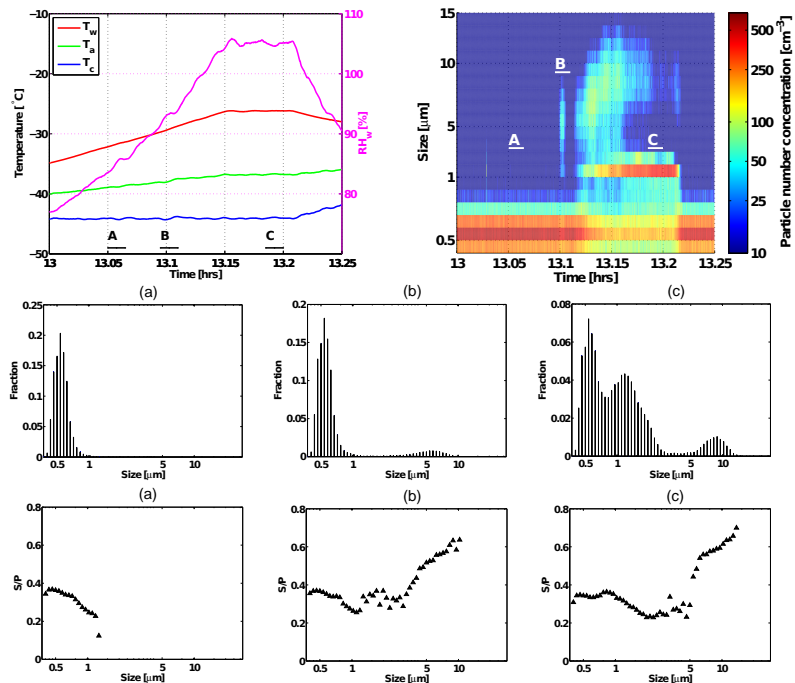Printer-friendly Version

Interactive Discussion

Figure 3. Deposition ice nucleation of viscous α-pinene SOA particles from 26.10.2014. Analogously to Fig. 1, the top left panel shows the SPIN wall and lamina temperatures and the RH_w as a function of time, and the top right panel the particle number concentrations in different size bins. Also here, bars A, B, C in the upper panels correspond to the time intervals from which the normalised SPIN OPC particle number size distributions and median values of polarisation-equivalent S/P ratios are shown in the lower panels. Panel **(a)** shows the 550 nm seed aerosol and panel **(b)** depicts seeds and ice crystals at water subsaturated conditions. A prominent liquid droplet mode can be seen in panel **(c)**, when homogeneous freezing was observed at water supersaturation. The size distributions are averaged over 54 s and correspond to the following times in the upper panels: **(a)** 13.05–13.065 h, **(b)** 13.095–13.11 h, **(c)** 13.185–13.2 h.

Title Page

Abstract | Introduction

Conclusions | References

Tables | Figures

|◄ | ►|

◄ | ►

Back | Close

Full Screen / Esc

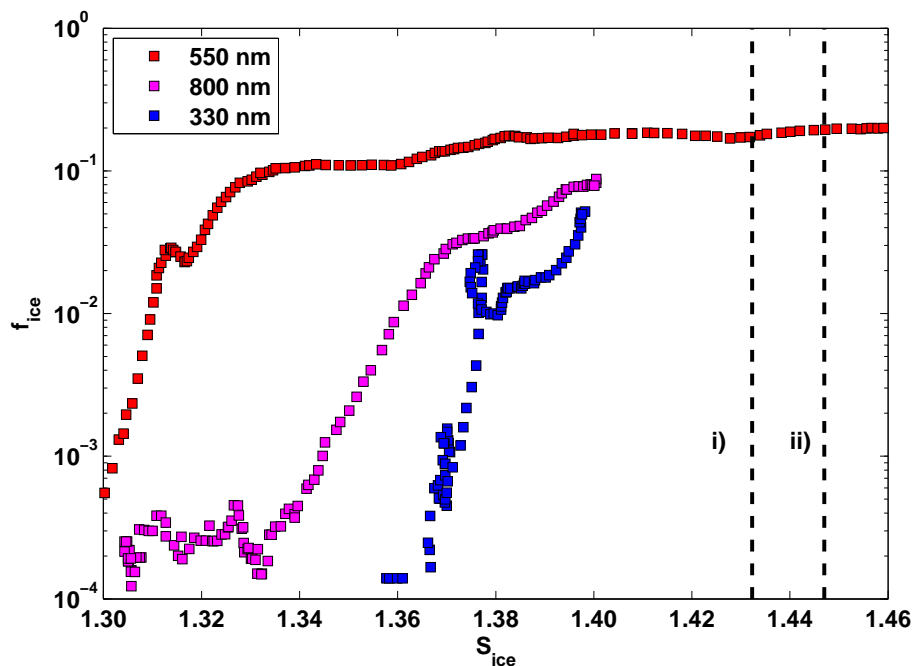Printer-friendly Version

Interactive Discussion

Figure 4. Examples of frozen fractions of viscous α-pinene SOA obtained with SPIN as a function of the ice saturation ratio S_{ice}. The blue squares correspond to seed aerosol of 330 nm, formed at $-38\,°C$, the red squares are the 550 nm particles, formed at $-20\,°C$, and the magenta squares are 800 nm particles, formed at $-10\,°C$. At the time of ice formation, the aerosol sample temperature inside SPIN was kept at approximately $-37.7\,°C$ for 330 nm particles; for 550 nm particles the temperature was at $-38.1\,°C$ and for 800 nm particles at $-37.0\,°C$. The black dashed vertical lines correspond to water saturation at (i) $-37\,°C$ and (ii) $-38\,°C$. Ice activation thresholds (1, 0.1 %) were determined from similar ice activation graphs.
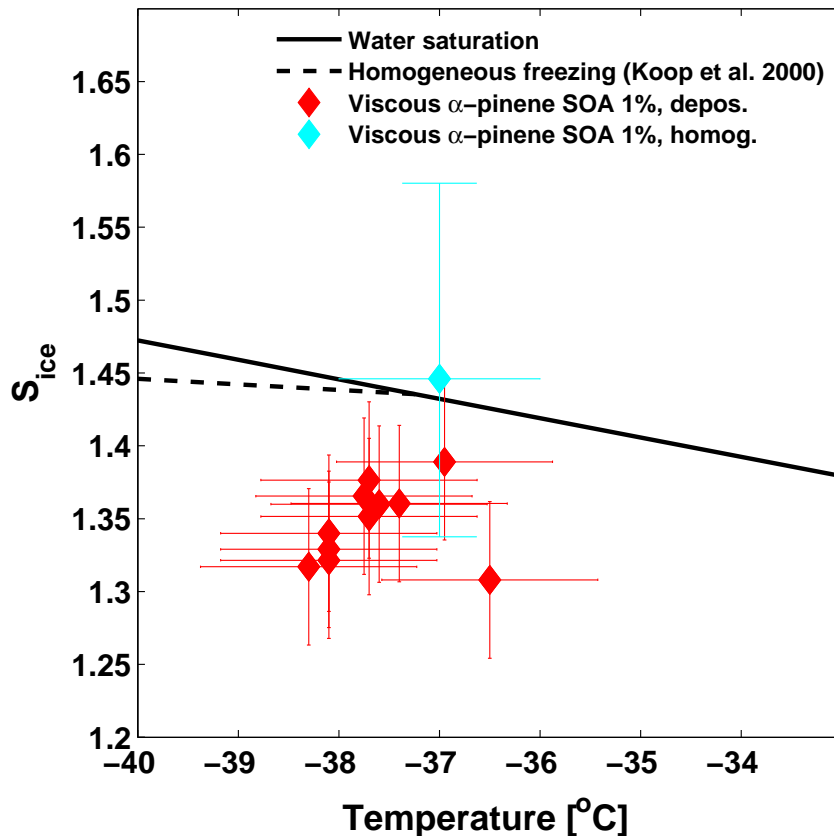
Figure 5. Ice nucleation onsets (1 % activation) for α-pinene SOA in the deposition (red diamonds) and homogeneous (cyan diamond) freezing mode. The error bars of the deposition nucleation data represent statistical 95 % confidence interval in both temperature and supersaturation, and are calculated from the standard deviation. Homogeneous freezing onset was observed only once, hence the error bars in supersaturation correspond to the theoretical maximum error calculated from the estimated instrumental temperature uncertainty.
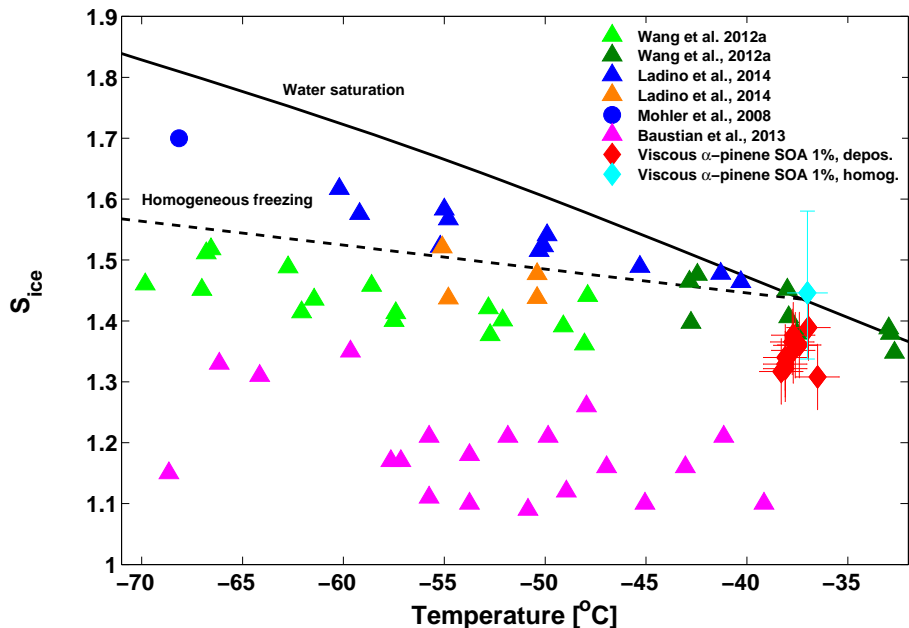
Discussion Paper | Discussion Paper | Discussion Paper | Discussion Paper

Title Page

Abstract | Introduction

Conclusions | References

Tables | Figures

|◄ | ►|

◄ | ►

Back | Close

Full Screen / Esc

Printer-friendly Version

Interactive Discussion

Figure 6. Comparison of ice nucleation onsets of different SOA species and proxies. The black solid line is the water saturation line and the black dashed line the Koop et al. (2000) homogeneous freezing line for 500 nm particles. The red and cyan diamonds represent the results of this study; the light and dark green triangles deposition nucleation and immersion freezing of naphthalene SOA from Wang et al. (2012); the magenta triangles deposition ice nucleation of sucrose from Baustian et al. (2013); the blue triangles ice nucleation of α-pinene SOA studied by Ladino et al. (2014) and the orange triangles pre-cooled α-pinene SOA from the same study; and the blue circle depicts the homogeneous freezing of pure α-pinene SOA reported by Möhler et al. (2008).

Title Page

Abstract · Introduction

Conclusions · References

Tables · Figures

|◄ · ►|

◄ · ►

Back · Close

Full Screen / Esc
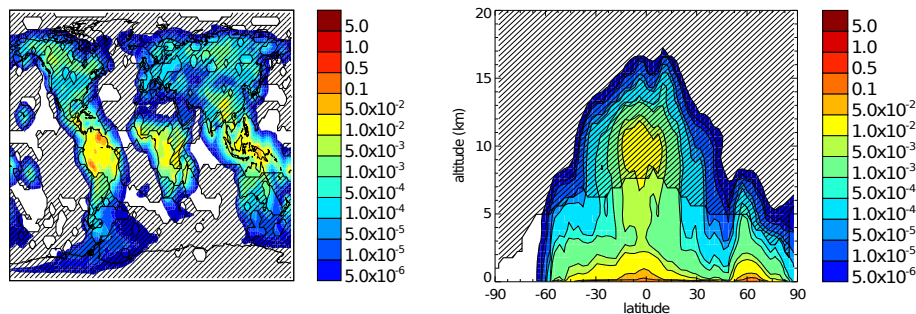
Printer-friendly Version

Interactive Discussion

Figure 7. GLOMAP model predictions of mean annual concentrations of condensible oxidation products of monoterpenes, SORG. The concentrations shown by the colourscale are in parts per trillion with respect to mass (pptm). The hatched areas represent the zones where the SOA particles could exist in a highly viscous or amorphous phase state in the upper troposphere and potentially affect cirrus cloud formation through ice nucleation. The calculations for these zones are based on the theoretical estimate of generic SOA glass transition temperature as a function of relative humidity presented by Koop et al. (2011). The left panel shows a global map of the mean annual concentrations of SORG at a sigma-pressure level corresponding to approximately 6900 m altitude from a simulation of the year 2000. In the right panel, annual zonal mean of global concentrations of SORG are plotted as a function of latitude and altitude.